





## ARTICLE OPEN



# Asian-Australian summer monsoons linkage to ENSO strengthened by global warming

Chenxi Xu<sup>1,2</sup> , S.-Y. Simon Wang<sup>3</sup> , Krishna Borhara<sup>3</sup>, Brendan Buckley<sup>4</sup>, Ning Tan<sup>1</sup>, Yaru Zhao<sup>1,5</sup> , Wenling An<sup>1</sup>, Masaki Sano<sup>6</sup> , Takeshi Nakatsuka<sup>6</sup> and Zhengtang Guo<sup>1,2</sup>

The El Niño-Southern Oscillation (ENSO) used to affect the Asian summer monsoon (ASM) and Australian summer monsoon (AusSM) precipitation in different ways but global warming may have changed it. This study built robust annual ASM (AusSM) precipitation reconstructions during 1588–2013 (1588–1999) to examine the ENSO-monsoon relationship and how it has changed. During the period of 1588–1850 when natural climate variability was dominant, the ENSO-monsoon and inter-monsoon relationship was weak and non-stationary. Since 1850, however, both the inter-monsoon and ENSO-monsoon relationships saw an enhancement and this trend has been persistent to the present day, suggesting the influence of anthropogenic climate warming. Further analysis of climate model projections found that global warming can strengthen the ENSO-monsoon association that, subsequently, acts to synchronize the ASM and AusSM variations.

*npj Climate and Atmospheric Science* (2023)6:8; <https://doi.org/10.1038/s41612-023-00341-2>

## INTRODUCTION

The Asian-Australian summer monsoon system includes Asian summer monsoon (ASM) in the northern hemisphere and Australian summer monsoon (AusSM) in the southern hemisphere. The Asian-Australian summer monsoon precipitation impact almost 3 billion people<sup>1</sup>. Previous studies based on observed and assimilated observational data showed that the El Niño-Southern Oscillation (ENSO) affected ASM and AusSM precipitation, as the El Niño can decrease both the June-September precipitation in Southeast Asia and the December-February precipitation in northern Australia through suppression of convective activity in the Indo-Pacific Warm Pool<sup>2</sup>. This ENSO effect caused an in-phase ASM and AusSM variability at inter-annual time scale<sup>2,3</sup>. Regarding the future change, past studies reported inconsistent trends in that global warming may either enhance, weaken, or maintain the teleconnection relationship between ENSO and ASM-AusSM<sup>1,4,5</sup>.

One complicating factor in the change of ENSO-monsoon association concerns the marked inter-decadal variation, which was shown in the relationship between ENSO and ASM-AusSM during the last century<sup>6,7</sup>. This factor can mask the effect of anthropogenic forcing<sup>4,6</sup>. As a result, the ASM-ENSO relationship is non-stationary at decadal time scale even though the AusSM-ENSO relationship has been stable since the 1950s<sup>8</sup>. The intrinsic inter-decadal ENSO variability may also affect the ENSO teleconnection<sup>9</sup>, further complicating the monsoonal response. Previous ENSO-monsoon studies using paleoclimate data mainly focused on the regional precipitation rather than the precipitation covering the whole ASM and AusSM region<sup>10,11</sup>, making the investigation of the overall ENSO effect difficult.

Does the anthropogenic global warming affect ENSO-ASM/AusSM relationship? Here, we reconstruct ASM and AusSM precipitation with annual-resolution during the period of 1588–2013/1588–1999 and compare ENSO-monsoon and ASM-AusSM relationship before

and after the emergence of global warming signal. The results reveal enhanced ASM/AusSM-ENSO and ASM-AusSM relationship after global warming.

## RESULTS

### ASM and AusSM precipitation reconstruction

By using a newly developed tree ring oxygen isotope chronology in Myanmar (Supplementary Fig. 1) and 6 existing annual-resolved records<sup>12–17</sup> across the monsoon Asia (Fig. 1), we reconstructed ASM precipitation for the period of 1588–2013 (Fig. 2a). The Myanmar samples of *Pinus kesiya* come from 128 trees collected at Nat-ma-taung National Park in the Chin Hills region of western Myanmar (B.M. Buckley, personal communication). Six trees with relatively wide rings and old age were selected for oxygen isotope analysis, and six tree ring cellulose oxygen isotope ( $\delta^{18}\text{O}_c$ ) time series were significantly correlated and were averaged to produce the regional chronology (Supplementary Fig. 1). These seven records in monsoonal Asia have been shown to reflect the monsoon-season rainfall locally, which is also significantly correlated with the ASM precipitation (Supplementary Table 1). Here, the reconstructed ASM precipitation was based on the nested composite-plus-scale method<sup>18</sup>. For the AusSM precipitation (Fig. 2b), we used three regional precipitation reconstructions<sup>19</sup> during the period of 1588–1999 (Supplementary Table 2).

The ASM/AusSM precipitation reconstruction as presented here (Fig. 2) passes the rigorous calibration and verification tests used in dendroclimatology (Supplementary Figs. 4, 5), and the correlation coefficient between reconstructed and observed ASM precipitation during the period of 1901–1950 is 0.7, which indicates the observed ASM precipitation is robust to some extent. The ASM/AusSM precipitation reconstruction explains 53%/41% of the variance ( $r = 0.73/0.64$ ,  $n = 113$ ,  $p < 0.001$ ) during

<sup>1</sup>Key Laboratory of Cenozoic Geology and Environment, Institute of Geology and Geophysics, Chinese Academy of Sciences, Beijing 100029, China. <sup>2</sup>CAS Center for Excellence in Life and Paleoenvironment, Beijing 100044, China. <sup>3</sup>Department of Plants, Soils, and Climate, Utah State University, Logan, UT 84322, USA. <sup>4</sup>Tree Ring Lab, Lamont-Doherty Earth Observatory, Columbia University, Palisades, NY, USA. <sup>5</sup>College of Earth Sciences, University of Chinese Academy of Sciences, Beijing, China. <sup>6</sup>Graduate School of Environment Studies, Nagoya University, Nagoya 464-8601, Japan. ✉email: cxxu@mail.iggcas.ac.cn

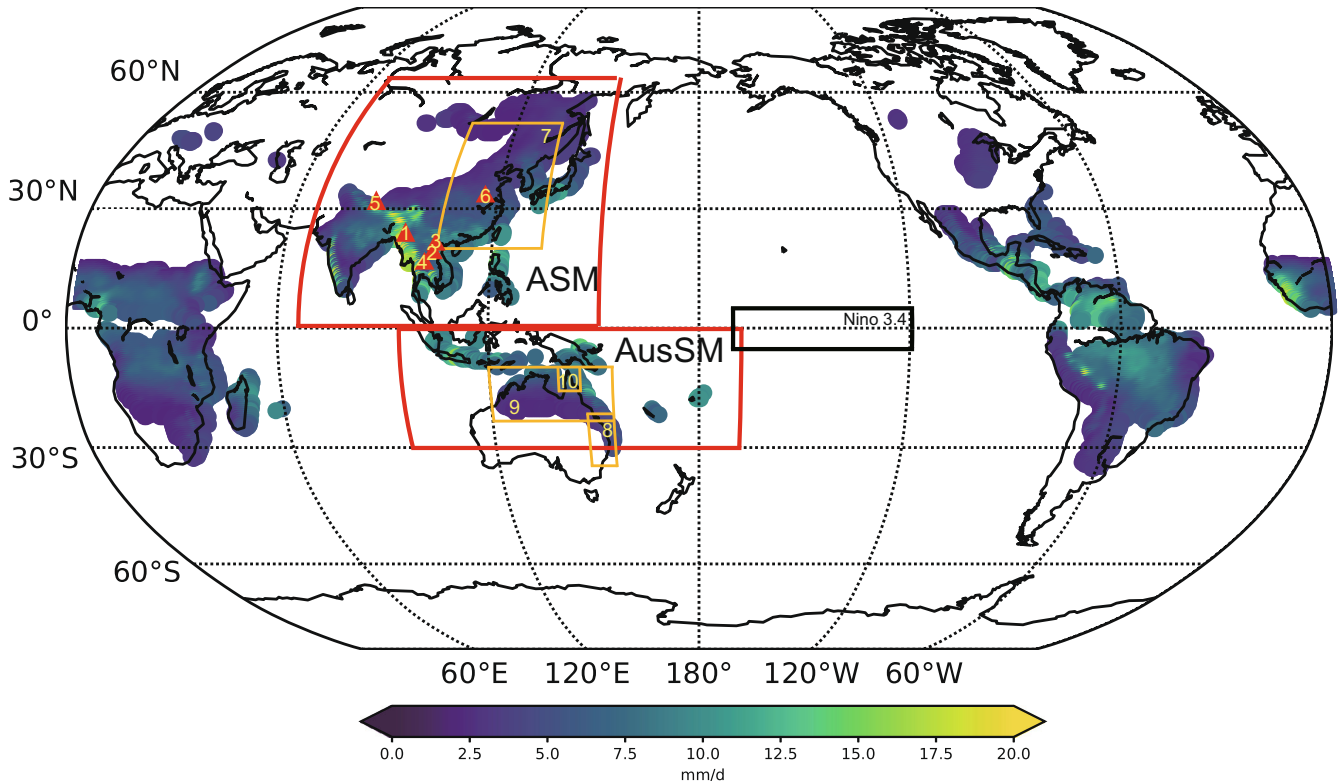


**Fig. 1 Global monsoon domain and 10 records used for ASM and AusSM precipitation reconstruction.** The global monsoon domain (shading area) which was calculated using precipitation data from CRU TS4.01 and GPCP 2018 during the period of 1901–2016 based on the definition in the previous study<sup>1</sup>. Red boxes indicate ASM and AusSM domain. Location of the 10 records (red triangles and orange boxes) for ASM and AusSM precipitation reconstruction. Red triangles indicate the tree ring oxygen isotope chronologies and orange boxes indicate regional precipitation reconstruction in previous study; black box indicates Niño 3.4 area.

the instrumental period of 1901–1999. In terms of regional representation, the reconstructed ASM precipitation showed significant and positive correlations with May–September precipitation in India, East China, southeast Asia, and Maritime continent. The reconstructed AusSM precipitation showed significant and positive correlations with Nov–Mar precipitation in Eastern Australia. These are consistent with the observations (Supplementary Fig. 6), and ASM/AusSM precipitation reconstruction are considered robust.

#### ASM-AusSM relationship at inter-annual scale

To examine the fluctuation in the ENSO-monsoon association, we computed the 31-year running correlations between the ASM/AusSM precipitation and annual ENSO index (Fig. 3). An enhanced ENSO-monsoon relationship since 1850 was observed. The relationship between ASM and annual sea surface temperature (SST) in eastern Pacific (which is produced by averaging two annual SST reconstructions; see supplementary materials) is weak during the period of 1588–1850, with a correlation coefficient of  $-0.11$  (Fig. 3a). However, the ASM-ENSO relationship started to enhance since 1850, and their correlation coefficient became a significant  $-0.64$ . We note that the relationship between AusSM and annual ENSO index reconstruction did fluctuate during the period of 1588–1850 but it too has strengthened since 1850 ( $r = -0.7$ ). Such an enhanced ASM-/AusSM-ENSO relationship is also evident based on boreal winter ENSO index that is produced by averaging four winter SST reconstructions in eastern Pacific (Supplementary Fig. 8a). The correlation coefficient between the ASM precipitation with boreal winter ENSO index was  $-0.25$  during the period of 1588–1850 and increased to  $-0.63$  after 1850. The correlation coefficient between AusSM and winter ENSO index fluctuated during the period of 1588–1850 and then

strengthened after 1850 to  $-0.73$  (Supplementary Fig. 8a). Similar tendencies since 1850 also exist between individual ENSO index reconstructions and the reconstructed ASM/AusSM precipitation (Supplementary Tables 3, 4).

Before 1850, ASM and AusSM did not exhibit a consistent relationship; for example, there were in-phase relationships during 1588–1650, 1720–1770 and 1800–1850 associated with out-phase relationships in 1650–1700 and 1770–1790 (Fig. 3b), depicting an unsynchronized inter-monsoon variation. Since 1850, consistent in-phase relationship became the norm between ASM and AusSM with an increasing trend reaching an unprecedented level in the late 20th century. The correlation coefficient between the reconstructed ASM precipitation and AusSM precipitation was 0.14 during 1588–1850, but it reached 0.54 after 1850, a substantial increase. Such a strengthened ASM-AusSM relationship at inter-annual time scale is verified in the wavelet coherence analysis (Fig. 2c), which indicates a robust in-phase relationship from 1850 to 1999 between the two monsoons. The in-phase ASM-AusSM relationship during the modern era has been validated by meteorological data<sup>2</sup>.

#### ENSO-monsoon relationship

ENSO likely controls the in-phase ASM-AusSM relationship, as the El Niño reduces convection in Western Pacific warm pool and subsequently decreases the ASM and AusSM precipitation<sup>2,3</sup>. ENSO variability appeared to have modulated the ENSO-ASM relationship at interdecadal scales during the past 100 years<sup>7</sup>. Therefore, an amplified ENSO variability due to global warming, as is shown in the increased standard deviation of ENSO index (Fig. 3c & Supplementary Fig. 8b), may be driving the enhanced ENSO-monsoon relationship. This process is possible because the increasingly energized convection in the Western Pacific warm

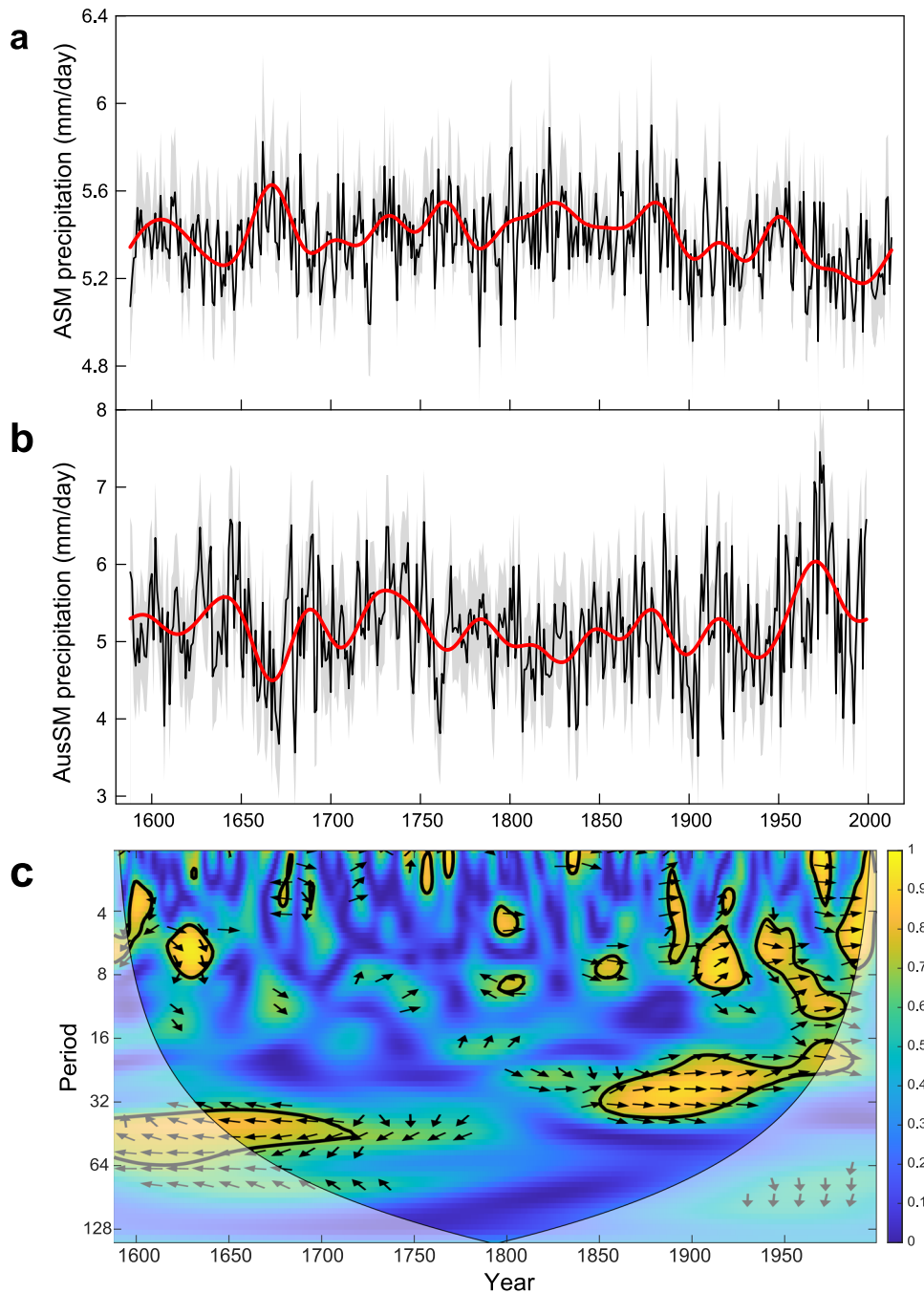


**Fig. 2** ASM and AusSM precipitation variations during the last 400 years. **a** The ASM and **(b)** AusSM precipitation reconstruction for the past 426 years (AD 1588–2013) (black line;  $\pm 1$  RMSE, grey shading) and 30-year low-pass-filtered (red line). **c** Wavelet coherence between ASM and AusSM precipitation.

pool can affect the ASM and AusSM precipitation and, in turn, create a seemingly in-phase relationship between ASM and AusSM. Using 20 CMIP5 climate models, previous research<sup>1</sup> projected an increase in the AASM-ENSO relationship under anthropogenic global warming, a finding that echoes the enhanced ENSO teleconnection regardless of the uncertainty in how ENSO itself would change<sup>20</sup>.

Using the newer generation of climate models (CMIP6), we examined the Asian-Australian summer monsoon-ENSO relationship through the detection-and-attribution experiments of the CMIP6 simulations (see Methods). Following the analysis of Fig. 3, we computed the 31-year sliding correlations between the

CMIP6's ASM and AusSM precipitation; this was simulated from the greenhouse gas forcing (GHG) runs and the natural-only forcing (NAT) runs. As shown in Fig. 4a, the simulated ASM and AusSM correlations exhibit a marked uptrend in GHG and a weak downward trend in NAT. This result echoes Fig. 3b and lends support to the suspected effect of global warming on the increasingly “coordinated” interannual variation of the two monsoons despite their different seasons.

By analyzing the individual monsoon's connection with ENSO, the sliding correlations between the ASM precipitation and the averaged Niño 3.4 SST index of the adjacent two winters show a marked divergence between the GHG and NAT runs around the

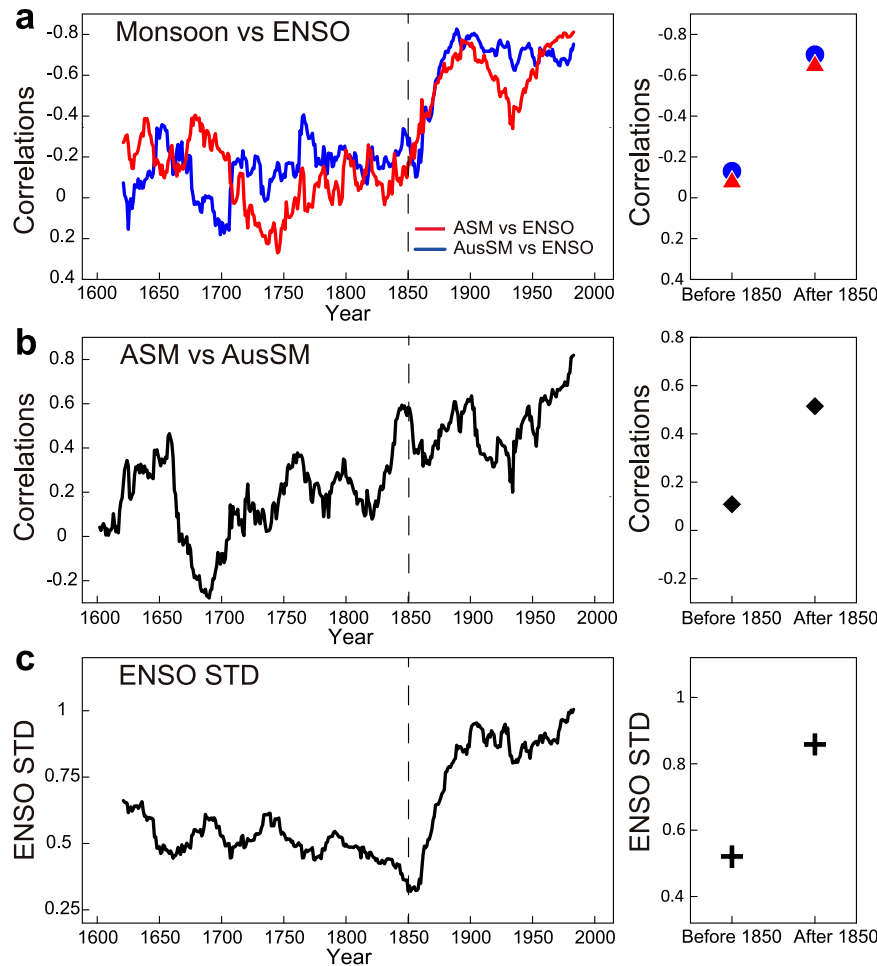


**Fig. 3** ASM-AusSM and monsoon-ENSO relationship during the last 400 years. **a** 31-year running correlations between ASM (red line)/AusSM (blue line) precipitation and ENSO. **b** 31-year running correlations between ASM and AusSM precipitation. **c** 31-year running standard deviation of reconstructed annual ENSO index during the period of 1588–1999. Correlation coefficients of monsoon-ENSO/inter-monsoon and standard deviation of reconstructed annual ENSO index at the period of 1588–1850 and 1851–1999 were shown in right side.

1950s' (Fig. 4b), with an upward trend in the GHG runs leveling off after the 1980s. The correlations between the AusSM precipitation and concurrent Niño 3.4 SST index also show a similarly divergent trends of the GHG and NAT runs (Fig. 4c), albeit the GHG run shows a more gradual uptrend than that of ASM. This too indicates that greenhouse gases have a robust effect on the ASM-AusSM-ENSO relationships that contribute to the increased coherency of the two large monsoon systems, supporting the finding of<sup>1</sup> with an updated climate modeling evidence.

#### ASM-AusSM relationship at decadal to multidecadal timescales

In addition to enhanced in-phase relationship between ASM and AusSM at inter-annual timescales since 1850, ASM-AusSM relationship at decadal to multidecadal timescales changed since 1850. Wavelet coherence analysis reveals anti-phase relationship between ASM and AusSM at interdecadal timescales from 1588 to 1800, while in-phase relationships from 1850 to 1999 (Fig. 2c). Specifically, 1650–1680 is high precipitation period for ASM and low precipitation period for AusSM, when Atlantic multidecadal oscillation (AMO)<sup>21</sup> is in negative phase (Fig. 5). The periods of 1620–1650, 1780–1800 saw low precipitation period for ASM and high precipitation period for AusSM, when AMO is in positive phase (Fig. 5). Therefore, AMO may cause anti-phase ASM-AusSM relationship as indicated by positive AMO-ASM relationship ( $r = 0.52$ ) and negative AMO-AusSM relationship ( $r = -0.33$ )

during the period of 1588–1850. AMO exerted influences on Intertropical Convergence Zone (ITCZ) through altering inter-hemisphere temperature gradient, and then affected ASM-AusSM relationship. Therefore, when positive-phase AMO increases temperature in northern Atlantic and inter-hemisphere temperature gradient, shifting the ITCZ northward while causing the ASM (AusSM) precipitation to increase (decrease), vice versa<sup>22</sup>. The anti-phase relationship between ASM and AusSM is also found at millennial time scales<sup>23,24</sup>, and the anti-phase relationship between northern and southern hemisphere monsoon is evident at orbital time scale<sup>25</sup>.

Since 1850, however, the anti-phase relationship between ASM and AusSM vanished, while an in-phase relationship between ASM and AusSM emerged. The increased ENSO variability and associated teleconnection may have overshadowed the meridional shift of the ITCZ effect and replaced it with the zonal variation of the ENSO teleconnection since 1850. Regarding the latter forcing, a type of ENSO-forced low-frequency variation called the Interdecadal Pacific oscillation (IPO)<sup>26</sup> may contribute to the enhanced in-phase relationship between ASM and AusSM since 1850 as shown in Figs. 2c, 5. We found that the correlation coefficients between ASM/AusSM and IPO from 1588–1850 were  $-0.41/-0.07$ , and they became  $-0.73/-0.29$  during 1851–1999. These results suggest that an enhanced Pacific Walker circulation effect may have undertaken the Hadley circulation effect on influencing the two monsoon systems.



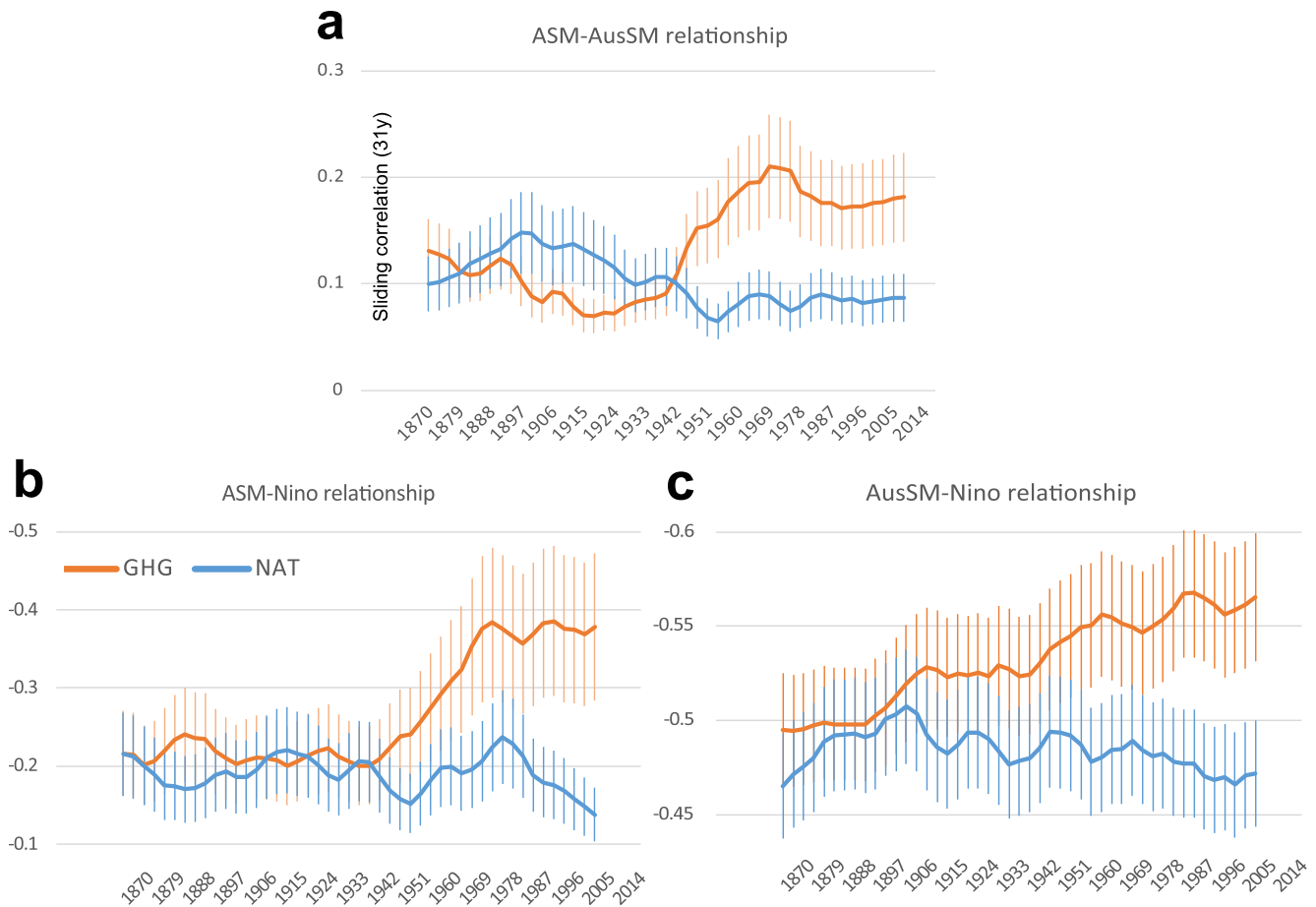


**Fig. 4** ASM-AusSM and monsoon-ENSO relationship from CMIP 6. **a** 31-year running correlations between ASM and AusSM precipitation. **b** 31-year running correlations between ASM precipitation and ENSO. **c** 31-year correlations between AusSM and Nino from CMIP 6. Error bars represent two standard deviations from the mean. The running correlations are centered. The number of models/members used here is (a) 26, (b) 28, and (c) 26 out of the 50 total models listed in Supplementary Table 5 (see Methods).

### ASM-AusSM relationship at centennial timescales and other forcings impacts

ASM showed an increasing trend during the period of 1588–1850 and a decreasing trend since 1850 (which is similar with rainfall reconstruction in Mexico<sup>27</sup>), while AusSM precipitation revealed a decreasing trend during the period of 1588–1800 and an increasing trend since 1800 (Fig. 6a). ASM and AusSM showed anti-phase variation at centennial time scale, which indicate that ITCZ shifting dominated the inter-relationship of ASM and AusSM. During the period of 1588–1800, total solar irradiance (TSI) and atmosphere CO<sub>2</sub> concentration increased, although the increasing trend is slight (0.1 W/m<sup>2</sup> per 100 years for TSI, and 2 ppmv per 100 years, Fig. 6d)<sup>28,29</sup>. These external forcing changes resulted in increased northern hemisphere land air temperature<sup>30</sup>, which should increase north-south hemisphere thermal contrast and ITCZ northward shift and subsequently strengthen ASM (weaken AusSM).

Estimated aerosol production in Europe and North America experienced a rapid increase since 1850 (Fig. 6c)<sup>31</sup>, which is consistent with sulphates variations in Greenland ice core<sup>32</sup>. Anthropogenic sulfate aerosol mostly located at Europe, North America, and Asia, therefore cooling the northern hemisphere while decreasing the inter-hemisphere thermal contrast. These subsequently led to the southward shift of ITCZ and reduced ASM/increased AusSM precipitation. Observed and simulated results showed that increased anthropogenic sulfate aerosol caused the southward shift of tropical precipitation in the late 20th century<sup>33</sup>.

Further analysis using multiple coupled climate models forced by the anthropogenic aerosols and idealized AGCM experiments showed that anthropogenic aerosols caused summer precipitation decrease in most of Asian monsoon, North Africa and part of north American monsoon since 1850<sup>34</sup>. Aerosol forcing is the more efficient external forcing in changing tropics precipitation than solar and GHG<sup>35</sup>, which is why it appears to have stronger influences on ASM and AusSM precipitation than solar and GHG since 1850.

Large-scale human agricultural activities resulted in deforestation, i.e. the conversion of forests to cropland and pasture, and this has led to regional climate changes via biochemical and biophysical effects<sup>36</sup>. Global (NH summer monsoon regions) cropland and pasture area increased rapidly from 12.8(5.1) to 49.6(16.8) million km<sup>2</sup> during the period of 1850–2000 which accounts for 34.9% global land area (Fig. 6e), and the increasing rate is high prior to 1800<sup>37</sup>. Albedo in cropland and pasture area is higher than forest, so increased global cropland and pasture area resulted in cooling and reduced inter-hemisphere thermal contrast, and these could shift the ITCZ as well. Southward shift of ITCZ and precipitation decrease in northern hemisphere monsoon area were found in most deforestation simulations<sup>36</sup>. Deforestation in monsoon area resulted in decreased evapotranspiration and subsequent decrease in the recycled component of precipitation<sup>38</sup>, and this led to a weakening of the monsoon circulation<sup>39</sup>. Therefore, since 1850 CE, anthropogenic aerosols and land cover changes caused ITCZ southward shift and decreased ASM/increased AusSM precipitation since 1850 CE (Fig. 6a).

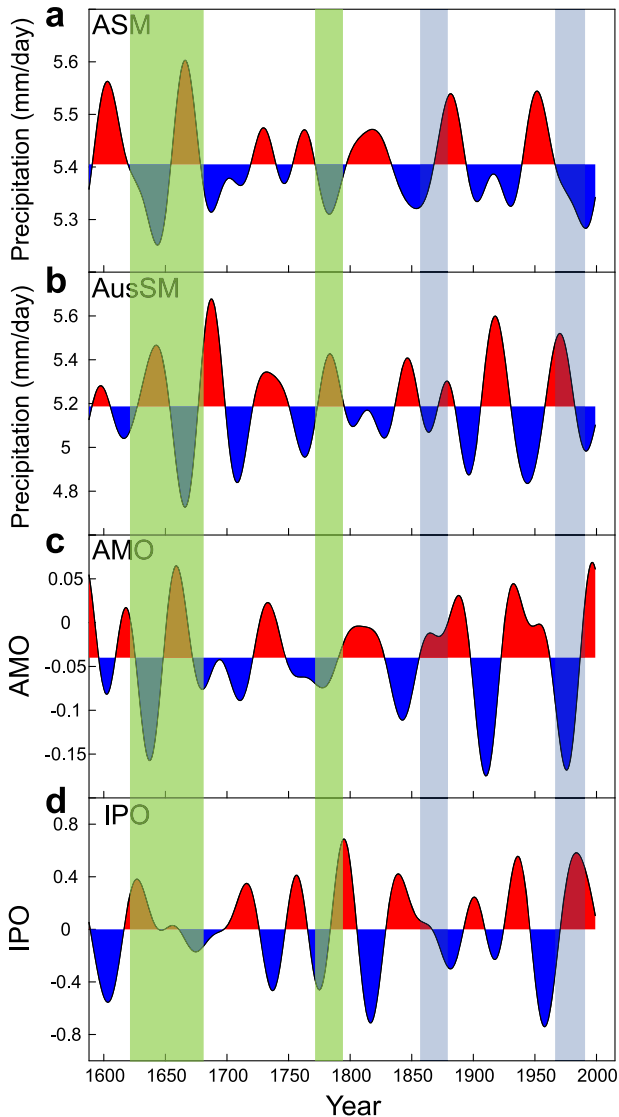


**Fig. 5 Multi-decadal variations of monsoon precipitation and internal variability.** **a** ASM precipitation. **b** AusSM precipitation. **c** AMO<sup>21</sup>. **d** IPO<sup>60–62</sup>.

## DISCUSSION

This study was intrigued by the contradictory trends in the monsoon-ENSO relationship revealed from past studies. Some authors reported a weakening relationship between the Asian/Indian Monsoon and ENSO<sup>4,6,7,40,41</sup>, which contradicts the finding of<sup>1</sup>. The literature's contradictory results were caused by inconsistent data sources and the tendency of coupled climate models to favor an El Niño response in the warming scenarios; that is, as an enhanced El Niño response weakens the Walker circulation in the long run, it would weaken its association with the ASM-AusSM rainfall as well. We also note that other extratropical factors also can influence the ENSO-monsoon relationship. For example, poleward migration and jet stream strengthening over the North Atlantic can shift the meridional temperature gradient required for the development of the Indian monsoon, and this phenomenon can weaken the ENSO-monsoon association as well<sup>41</sup>. Our CMIP6 analysis presented in Fig. 4 and the newer paleoclimate reconstruction lend support to other studies that found a strengthened variability of ENSO effects<sup>42</sup>.

The in-phase relationship of ASM and AusSM at inter-annual time scale started in the late 19th century and reached an

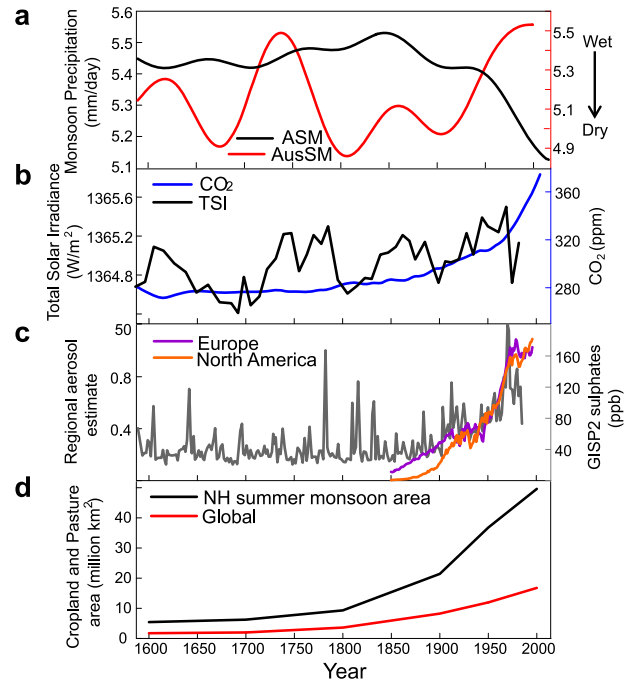


**Fig. 6 Centennial variations of monsoon and external forcings.** **a** Centennial variations of ASM (black line) and AusSM (red line) precipitation. **b** Time series of total solar irradiance (28, black line) and atmospheric CO<sub>2</sub> concentration (29, blue line). **c** Regional aerosol estimate (30, purple and orange lines) and GISP2 sulphates (31, gray line) in Greenland. **d** Northern Hemisphere summer monsoon (black line) and Global (red line) cropland and Pasture area<sup>37</sup>.

unprecedented level of coherency in the 21st century, owing to the enhanced ENSO variability/teleconnection under the increased CO<sub>2</sub> emissions. With the increased ENSO variability projected in the future<sup>43</sup>, we may see a stronger ENSO-monsoon relationship with the increased possibility of monsoon extremes<sup>44</sup> and resultant floods and droughts in the monsoonal regions.

## METHODS

### A new tree ring cellulose oxygen isotope record in Myanmar

*Pinus kesiya* samples from 128 trees were collected at Nat-ma-taung National Park (21°30'N, 93°46'E, 2000–2800m a.s.l.), Chin Hills, Myanmar in 2014. Samples were cross-dated in Tree Ring Lab, Lamont-Doherty Earth Observatory, Columbia University and the results were checked by COFECHA. Six trees (MNPk 12c, 19a, 113b, 114a, 115c, 123b) with relative wide rings and old age were selected for oxygen isotope analysis to produce the long oxygen isotope chronology. Cellulose extraction was conducted using wood plate samples<sup>45</sup>. Tree ring cellulose oxygen isotope ( $\delta^{18}\text{O}_c$ ) measurements were determined by an isotope ratio mass (Delta V Advantage, Thermo Scientific) at the Research Institute for Humanity and Nature, Japan. The analytical uncertainty for repeated measurements of cellulose was approximately  $\pm 0.18\text{‰}$  ( $n = 260$ ).  $\delta^{18}\text{O}_c$  from six trees are shown in Supplementary Fig. 1a. The inter-trees correlation (RBAR) is range from 0.56 to 0.68 (Supplementary Fig. 1b), which reflect their common response to climate. Six  $\delta^{18}\text{O}_c$  time series were averaged to produce the regional  $\delta^{18}\text{O}_c$  chronology (Supplementary Fig. 1c) for the period 1672–2013, since mean and standard deviation for each  $\delta^{18}\text{O}_c$  time series are similar. Climatic response indicates that MNPk  $\delta^{18}\text{O}_c$  chronology is correlated with regional May–October precipitation (Supplementary Fig. 2).

### Definition of monsoon domain and monsoon intensity

The global monsoon domain is defined by the annual range of precipitation exceeding 2.0 mm/day and the local summer precipitation (May–September) exceeding 55% of the annual precipitation<sup>46</sup>. Annual range is defined as local summer precipitation minus local winter precipitation, and local summer is defined from May to September, and local winter is defined from November to March<sup>46</sup>. Precipitation from CRU TS4.01<sup>47</sup> and GPCC V2018<sup>48</sup> with 0.5° grid resolution during the period of 1901–2016 were averaged to calculate monsoon domain and monsoon intensity. Monsoon domain in land were shown in Fig. 1, which is similar with results from previous study<sup>2</sup> based on the data set from Global Precipitation Climatology Project (GPCP) and Climate Prediction Center merged analysis of precipitation (CMAP). May–September Asian and Australian summer monsoon precipitation, which was averaged over the land summer monsoon rainfall at Asian and Australian summer monsoon domain respectively<sup>46</sup> (Fig. 1), were used for calibration and verification of monsoon precipitation reconstruction.

### Asian summer monsoon precipitation and Australia summer monsoon reconstruction

Six tree ring cellulose oxygen isotope chronologies with accurate dating and annual resolution from Asia monsoon area and one regional precipitation record in Eastern China were used for Asian summer monsoon precipitation reconstruction (Supplementary Table 1). Seven records in monsoonal Asia have been proved to record regional monsoon season rainfall, which showed significant correlations with ASM precipitation (Supplementary Table 1). Three regional precipitation records covering the East Coast, Monsoonal North and Wet tropics in Australia has positive correlations with Australia summer monsoon precipitation, were used for AusSM precipitation reconstruction (Supplementary Table 2).

A weighted and nested composite-plus-scale (CPS) approach<sup>49</sup> to reconstruct ASM and AusSM precipitation. Each record is robustly correlated with the observed ASM and AusSM precipitation records (Supplementary Table 1). Instrumental precipitation data increased rapidly after 1950s in Asia monsoon area<sup>50,51</sup>. Therefore, 1951–1999 was used as calibration period and 1901–1950 was used as verification period. The explained variance ( $r^2$ ), reduction of error (RE), and coefficient of efficiency (CE) were used to test the reliability of the ASM and AusSM precipitation reconstructions<sup>52</sup>, and the Root Mean Squared Error (RMSE) was used to characterize the uncertainty<sup>49</sup>. When CE that is the most rigorous statistic for reconstruction is higher than zero, reconstruction is robust<sup>52</sup>. For the ASM/AusSM precipitation reconstruction, seven/three records were weighted based on the correlation between the proxy record and the ASM precipitation during the calibration period of 1951–1999, and 11/3 nests reflect the changing number of available records on reconstructed skill and variance over time.

The ASM/AusSM precipitation reconstruction is highly correlated with observed ASM/AusSM precipitation based on the merged CRU and GPCC datasets ( $r = 0.78/0.65$ ) during the period of 1951–1999 (Supplementary Fig. 3). The ASM/AusSM precipitation reconstruction (Fig. 2) during the period of 1588–2013/1588–1999 passes the rigorous calibration and verification tests used in dendroclimatology (Supplementary Figs. 4, 5) and explains nearly 53%/41% of the variance during 1901–1999. In terms of regional representation, the reconstructed ASM precipitation showed positive correlations with May–September precipitation in India, East China, southeast Asia, and Maritime continent. The reconstructed AusSM precipitation showed positive correlations with Nov–Mar precipitation in Eastern Australia; these are consistent with the observations (Supplementary Fig. 6). The MTM spectrum analysis of ASM and AusSM precipitation indicates significant inter-annual and multi-decadal variations

(Supplementary Fig. 7). Wavelet coherence is used to evaluate the ASM–AusSM relationship at different time scales<sup>53,54</sup>.

### Climate proxy data

ENSO have great influence on ASM and AusSM precipitation. We produced two composite ENSO reconstructions to evaluate ENSO–monsoon relationship according to the seasonal of ENSO reconstructions. One composite ENSO reconstruction is produced by averaging four normalized ENSO reconstructions<sup>55–58</sup> which mainly focused on boreal winter SST variations in tropics Pacific and were reconstructed based on multi-proxies including corals, tree rings, ice cores etc. We termed this composite ENSO reconstruction as boreal winter ENSO index, the year of boreal winter ENSO indicated the SST variations mainly from previous November to current February. Another composite ENSO reconstruction is produced by averaging two normalized ENSO reconstructions<sup>49,59</sup> which mainly focused on annual SST variations in tropics Pacific and were reconstructed based on corals and ice core. We termed this composite ENSO reconstruction as annual ENSO index. There are no repetitive proxies used for composite ENSO index and ASM reconstruction. AusSM reconstruction is based on 102 records, while a few of them were used for previous ENSO reconstruction. We are confident that it does not affect the results because 1) the proportion of repetitive proxies is low, so their contribution on the AusSM variation is low; 2) some records showed very weak correlations with the ENSO index; and 3) even if these repetitive records disrupted the monsoon–ENSO relationship, the long-term monsoon–ENSO relationship should be stable after the composite.

A 9-year high-pass filter is used to extract inter-annual monsoon precipitation and explore monsoon–ENSO relationship<sup>54</sup>. A composite IPO reconstruction is produced by averaging three IPO reconstructions<sup>60–62</sup>. An synthesized AMO reconstruction based on a network of annual resolution records from North Atlantic region<sup>21</sup> were employed to evaluate AMO's influences on ASM and AusSM at multi-decadal scales. To extract multi-decadal variability of ASM, AusSM, IPO and AMO, A 30–70 years band-pass FFT filter were used.

Total solar irradiance (28, TSI), atmosphere CO<sub>2</sub> concentration<sup>29</sup>, aerosol production estimated using CO<sub>2</sub> emissions relative to 1992 levels for Europe and North America<sup>31</sup>, GISP2 total sulphate record<sup>32</sup> and long-term land use history<sup>37</sup> were used to compare with centennial changes of ASM and AusSM. The long-term changes of ASM and AusSM were extracted using a 100-year lowpass filter<sup>63</sup>.

### Climate models and grouping

To attribute the relationship change between the Asian summer monsoon and the Australian monsoon, and between each monsoon and ENSO, sliding correlations were obtained from three CMIP6 runs: all forcing simulations of the recent past (HIST), historical greenhouse-gas only simulations (GHG), and historical natural-only simulations (NAT) that consider aerosol and solar forcings only. We obtained 50 ensemble members for each run and the models used are summarized in Supplementary Table 5. It is difficult for models to produce the observed relationship of ENSO–monsoon in recent decades because external forcing is difficult to separate from internal variability<sup>64</sup> and models have many biases. The historical trends in the Pacific SST and atmospheric circulation pattern are heavily influenced by the predominant multi-decadal variability, which is *opposite* to what most climate models projected<sup>65</sup>. When performing multi-model large ensembles, such an opposite trend (compared to the projection) vanishes, leading to inconsistent results between the historical trends and the projected trends. The NAT-only forcing experiment resemble the millennium-scale simulations, albeit shorter in time. To be comparable with the GHG and HIST

forcing experiments, we adopted the NAT forcing even though the internal variabilities (such as what we observed in the past 50 years) would still cancel out. We further grouped models that have a more realistic performance in the HIST runs before the 20th century as a measure for selecting “better-performing” models for the subsequent analysis. We averaged two winters of the Niño 3.4 SST index to capture the longer-lasting ENSO events and their broad influences on the monsoons. The averaged index can eliminate the effect of the known quasi-biennial frequency of ENSO on the longer timescale.

Based on Fig. 3’s mean values during 1850–1900, we used the correlation range between 0 and 0.3 for the ASM-AusSM relationship, between  $-0.3$  and 0 for the ASM-ENSO relationship, and between  $-0.6$  and  $-0.4$  for the AusSM-ENSO relationship as the criteria to filter the model and ensemble members. In other words, only the HIST models/members that produce the 51-year correlation coefficients falling between the aforementioned ranges are chosen to produce Fig. 4. The numbers of the models/members used are described in the figure caption and Supplementary Table 5. The model selection process was adopted from previous studies<sup>66</sup>.

## DATA AVAILABILITY

The proxy data and ASM and AusSM precipitation reconstruction produced in this study are available in NOAA’s paleoclimate data repository (<https://www.ncdc.noaa.gov/paleo/study/>).

Received: 24 August 2022; Accepted: 8 February 2023;

Published online: 18 February 2023

## REFERENCES

- Wang, B., Yim, S.-Y., Lee, J.-Y., Liu, J. & Ha, K.-J. Future change of Asian-Australian monsoon under RCP 4.5 anthropogenic warming scenario. *Clim. Dyn.* **42**, 83–100 (2014).
- Hung, C.-w., Liu, X. & Yanai, M. Symmetry and asymmetry of the Asian and Australian summer monsoons. *J. Clim.* **17**, 2413–2426 (2004).
- Meehl, G. A. The annual cycle and interannual variability in the tropical Pacific and Indian Ocean regions. *Monthly Weather Rev.* **115**, 27–50 (1987).
- Li, X. & Ting, M. Recent and future changes in the Asian monsoon-ENSO relationship: Natural or forced? *Geophys. Res. Lett.* **42**, 3502–3512 (2015).
- Annamalai, H., Hamilton, K. & Sperber, K. R. The South Asian summer monsoon and its relationship with ENSO in the IPCC AR4 simulations. *J. Clim.* **20**, 1071–1092 (2007).
- Kumar, K. K., Rajagopalan, B. & Cane, M. A. On the weakening relationship between the Indian monsoon and ENSO. *Science* **284**, 2156–2159 (1999).
- Torrence, C. & Webster, P. J. Interdecadal changes in the ENSO-monsoon system. *J. Clim.* **12**, 2679–2690 (1999).
- Yim, S.-Y., Wang, B., Liu, J. & Wu, Z. A comparison of regional monsoon variability using monsoon indices. *Clim. Dyn.* **43**, 1423–1437 (2014).
- Cai, W. et al. Changing El Niño–Southern Oscillation in a warming climate. *Nat. Rev. Earth Environ.* **2**, 628–644 (2021).
- Xu, C. et al. Decreasing Indian summer monsoon on the northern Indian subcontinent during the last 180 years: Evidence from five tree-ring cellulose oxygen isotope chronologies. *Climate* **14**, 653–664 (2018).
- Lough, J. M. Tropical river flow and rainfall reconstructions from coral luminescence: Great Barrier Reef, Australia. *Paleoceanography* **22**, PA2218 (2007).
- Xu, C. et al. Increased variability of Thailand’s Chao Phraya river peak season flow and its association with ENSO variability: Evidence from tree ring  $\delta^{18}\text{O}$ . *Geophys. Res. Lett.* **46**, 4863–4872 (2019).
- Xu, C., Sano, M. & Nakatsuka, T. A 400-year record of hydroclimate variability and local ENSO history in northern Southeast Asia inferred from tree-ring  $\delta^{18}\text{O}$ . *Palaeogeogr., Palaeoclimatol., Palaeoecol.* **386**, 588–598 (2013).
- Sano, M. et al. May–September precipitation in the Bhutan Himalaya since 1743 as reconstructed from tree ring cellulose  $\delta^{18}\text{O}$ . *J. Geophys. Res.: Atmos.* **118**, 8399–8410 (2013).
- Sano, M., Xu, C. & Nakatsuka, T. A 300-year Vietnam hydroclimate and ENSO variability record reconstructed from tree ring  $\delta^{18}\text{O}$ . *J. Geophys. Res.: Atmos.* **117**, n/a–n/a (2012).
- Shi, F., Zhao, S., Guo, Z., Goosse, H. & Yin, Q. Multi-proxy reconstructions of May–September precipitation field in China over the past 500 years. *Climate* **13**, 1919–1938 (2017).
- Xu, C. et al. Early summer precipitation in the lower Yangtze River basin for AD 1845–2011 based on tree-ring cellulose oxygen isotopes. *Clim. Dyn.* **52**, 1583–1594 (2019).
- Esper, J., Cook, E. R. & Schweingruber, F. H. Low-frequency signals in long tree-ring chronologies for reconstructing past temperature variability. *Science* **295**, 2250–2253 (2002).
- Freund, M., Henley, B. J., Karoly, D. J., Allen, K. J. & Baker, P. J. Multi-century cool- and warm-season rainfall reconstructions for Australia’s major climatic regions. *Climate* **13**, 1751–1770 (2017).
- Simon Wang, S. Y., Huang, W. R., Hsu, H. H. & Gillies, R. R. Role of the strengthened El Niño teleconnection in the May 2015 floods over the southern Great Plains. *Geophys. Res. Lett.* **42**, 8140–8146 (2015).
- Wang, J. et al. Internal and external forcing of multidecadal Atlantic climate variability over the past 1,200 years. *Nat. Geosci.* **10**, 512–517 (2017).
- Schneider, T., Bischoff, T. & Haug, G. H. Migrations and dynamics of the inter-tropical convergence zone. *Nature* **513**, 45–53 (2014).
- Denniston, R. F. et al. North Atlantic forcing of millennial-scale Indo-Australian monsoon dynamics during the Last Glacial period. *Quat. Sci. Rev.* **72**, 159–168 (2013).
- Eroglu, D. et al. See-saw relationship of the Holocene East Asian–Australian summer monsoon. *Nat. Commun.* **7**, 1–7 (2016).
- Cheng, H., Sinha, A., Wang, X., Cruz, F. W. & Edwards, R. L. The Global Paleomonsoon as seen through speleothem records from Asia and the Americas. *Clim. Dyn.* **39**, 1045–1062 (2012).
- Power, S., Haylock, M., Colman, R. & Wang, X. The predictability of interdecadal changes in ENSO activity and ENSO teleconnections. *J. Clim.* **19**, 4755–4771 (2006).
- Medinaelzalde, M. et al. High resolution stalagmite climate record from the Yucatán Peninsula spanning the Maya terminal classic period. *Earth Planet. Sci. Lett.* **298**, 255–262 (2010).
- Delaygue, G. & Bard, E. An Antarctic view of Beryllium-10 and solar activity for the past millennium. *Clim. Dyn.* **36**, 2201–2218 (2011).
- Meure C.M. et al. Law Dome  $\text{CO}_2$ ,  $\text{CH}_4$  and  $\text{N}_2\text{O}$  ice core records extended to 2000 years BP. *Geophys. Res. Lett.* **33**, L14810 (2006).
- Ahmed, M. et al. Continental-scale temperature variability during the past two millennia. *Nat. Geosci.* **6**, 339–346 (2013).
- Robertson, A. et al. Hypothesized climate forcing time series for the last 500 years. *J. Geophys. Res.* **106**, 14783–14803 (2001).
- Zielinski, G. A. et al. Record of volcanism since 7000 B.C. from the GISP2 Greenland ice core and implications for the volcano-climate system. *Science* **264**, 948–952 (1994).
- Hwang, Y., Frierson, D. M. W. & Kang, S. M. Anthropogenic sulfate aerosol and the southward shift of tropical precipitation in the late 20th century. *Geophys. Res. Lett.* **40**, 2845–2850 (2013).
- Wang, H., Xie, S.-P., Kosaka, Y., Liu, Q. & Du, Y. Dynamics of Asian summer monsoon response to anthropogenic aerosol forcing. *J. Clim.* **32**, 843–858 (2019).
- Liu, F., Zhao, T., Wang, B., Liu, J. & Luo, W. Different Global Precipitation Responses to Solar, Volcanic, and Greenhouse Gas Forcings. *J. Geophys. Res.* **123**, 4060–4072 (2018).
- Devaraju, N., Bala, G. & Nemani, R. Modelling the influence of land-use changes on biophysical and biochemical interactions at regional and global scales. *Plant Cell Environ.* **38**, 1931–1946 (2015).
- Klein Goldewijk, K., Beusen, A., Van Drecht, G. & De, M. Vos, The HYDE 3.1 spatially explicit database of human-induced global land-use change over the past 12,000 years. *Glob. Ecol. Biogeogr.* **20**, 73–86 (2011).
- Paul, S. et al. Weakening of Indian Summer Monsoon Rainfall due to Changes in Land Use Land Cover. *Sci. Rep.* **6**, 32177 (2016).
- Fu, C. Potential impacts of human-induced land cover change on East Asia monsoon. *Global Planetary Change* **37**, 219–229 (2003).
- Krishnamurthy, V. & Goswami, B. N. Indian monsoon–ENSO relationship on interdecadal timescale. *J. Clim.* **13**, 579–595 (2000).
- Chang, C., Harr, P. & Ju, J. Possible roles of Atlantic circulations on the weakening Indian monsoon rainfall–ENSO relationship. *J. Clim.* **14**, 2376–2380 (2001).
- Cai, W. et al. Butterfly effect and a self-modulating El Niño response to global warming. *Nature* **585**, 68–73 (2020).
- Cai, W. et al. Increased ENSO sea surface temperature variability under four IPCC emission scenarios. *Nat. Clim. Change* **12**, 228–231 (2022).
- Buckleby, B. M., Fletcher, R., Wang, S.-Y. S., Zottoli, B. & Pottier, C. Monsoon extremes and society over the past millennium on mainland Southeast Asia. *Quat. Sci. Rev.* **95**, 1–19 (2014).
- Xu, C., Zheng, H., Nakatsuka, T. & Sano, M. Oxygen isotope signatures preserved in tree ring cellulose as a proxy for April–September precipitation in Fujian, the subtropical region of southeast China. *J. Geophys. Res.: Atmos.* **118**, 12,805–812,815 (2013).



46. Wang, B. et al. Northern Hemisphere summer monsoon intensified by mega-El Niño/southern oscillation and Atlantic multidecadal oscillation. *Proc. Natl Acad. Sci. USA* **110**, 5347–5352 (2013).
47. Harris, I., Jones, P. C. R. U. TS4. 01: Climatic Research Unit (CRU) Time-Series (TS) version 4.01 of high-resolution gridded data of month-by-month variation in climate (Jan. 1901–Dec. 2016). *J Centre Environ. Data Anal.* **25**, 1–18 (2017).
48. Schneider, U., Becker, A., Finger, P., Meyer-Christoffer, A., Ziese, M. J. GPCC Full Data Monthly Product Version 2018 at 0.5°: Monthly land-surface precipitation from rain-gauges built on GTS-based and historical data. (2018).
49. Tierney, J. E. et al. Tropical sea surface temperatures for the past four centuries reconstructed from coral archives. *Paleoceanography* **30**, 226–252 (2015).
50. Yatagai, A. et al. APHRODITE: Constructing a Long-Term Daily Gridded Precipitation Dataset for Asia Based on a Dense Network of Rain Gauges. *Bull. Am. Meteorol. Soc.* **93**, 1401–1415 (2012).
51. Sylla, M. B., Giorgi, F., Coppola, E. & Mariotti, L. Uncertainties in daily rainfall over Africa: assessment of gridded observation products and evaluation of a regional climate model simulation. *Int. J. Climatol.* **33**, 1805–1817 (2013).
52. Cook, E. R., Meko, D. M., Stahle, D. W. & Cleaveland, M. K. Drought reconstructions for the continental United States. *J. Clim.* **12**, 1145–1162 (1999).
53. Grinsted, A., Moore, J. C. & Jevrejeva, S. Application of the cross wavelet transform and wavelet coherence to geophysical time series. *Nonlinear Process. Geophys.* **11**, 561–566 (2004).
54. Wang, B., Yang, J., Zhou, T. & Wang, B. Interdecadal changes in the major modes of Asian–Australian monsoon variability: Strengthening relationship with ENSO since the late 1970s. *J. Clim.* **21**, 1771–1789 (2008).
55. Emile-Geay, J., Cobb, K. M., Mann, M. E. & Wittenberg, A. T. Estimating Central Equatorial Pacific SST Variability over the Past Millennium. Part I: Methodology and Validation. *J. Clim.* **26**, 2302–2328 (2013).
56. Li, J. et al. El Niño modulations over the past seven centuries. *Nat. Clim. Change* **3**, 822–826 (2013).
57. McGregor, S., Timmermann, A. & Timm, O. A unified proxy for ENSO and PDO variability since 1650. *Climate* **6**, 1–17 (2010).
58. Cook, E. et al. in *AGU Fall Meeting Abstracts*. (2008), vol. 2008, pp. PP24A-03.
59. Wilson, R. et al. Reconstructing ENSO: The influence of method, proxy data, climate forcing and teleconnections. *J. Quat. Sci.* **25**, 62–78 (2010).
60. Buckley, B. M. et al. Interdecadal Pacific Oscillation reconstructed from trans-Pacific tree rings: 1350–2004 CE. *Clim. Dyn.* **53**, 3181–3196 (2019).
61. Porter, S. E., Mosley-Thompson, E., Thompson, L. G. & Wilson, A. B. Reconstructing an interdecadal pacific oscillation index from a pacific basin-wide collection of ice core records. *J. Clim.* **34**, 3839–3852 (2021).
62. Vance, T., Roberts, J., Plummer, C., Kiem, A. & Van, T. Ommen, Interdecadal Pacific variability and eastern Australian megadroughts over the last millennium. *Geophys. Res. Lett.* **42**, 129–137 (2015).
63. Mann, M. E. Smoothing of climate time series revisited. *Geophys. Res. Lett.* **35**, L16708 (2008).
64. Deser, C., Phillips, A., Bourdette, V. & Teng, H. Uncertainty in climate change projections: the role of internal variability. *Clim. Dyn.* **38**, 527–546 (2012).
65. Sun, X. et al. Enhanced jet stream waviness induced by suppressed tropical Pacific convection during boreal summer. *Nat. Commun.* **13**, 1–10 (2022).
66. Promchote, P., Wang, S.-Y. S. & Johnson, P. G. The 2011 great flood in Thailand: Climate diagnostics and Implications from climate change. *J. Clim.* **29**, 367–379 (2016).

## ACKNOWLEDGEMENTS

This study is supported by the National Natural Science Foundation of China, Grant Number: 41888101, 42022059; the Key Research Program of the Institute of Geology and Geophysics (CAS Grant IGGCAS-201905), the Chinese Academy of Sciences (CAS) Pioneer Hundred Talents Program, CAS Youth Interdisciplinary Team (JCTD-2021-05), the Strategic Priority Research Program of the Chinese Academy of Sciences, Grant Number: XDB26020000. Simon Wang is supported by the U.S. Department of Energy research program under Award Number DE-SC0016605 and by NSF P2C2 award number - 1903721. Brendan Buckley acknowledges the support of NSF P2C2 award number AGS-2001949.

## AUTHOR CONTRIBUTIONS

Conceptualization: C.X., S.W.; Methodology: C.X., S.W., K.B., B.B., N.T., W.A., M.S., T.N.; Investigation: C.X., S.W., K.B., B.B., N.T., W.A., M.S.; Visualization: C.X., S.W., K.B., N.T.; Funding acquisition: C.X., S.W., B.B., Z.G.; Writing – original draft: C.X., S.W., K.B.; Writing – review & editing: C.X., S.W., K.B., B.B., N.T., W.A., M.S., T.N., Z.G.

## COMPETING INTERESTS

The authors declare no competing interests.

## ADDITIONAL INFORMATION

**Supplementary information** The online version contains supplementary material available at <https://doi.org/10.1038/s41612-023-00341-2>.

**Correspondence** and requests for materials should be addressed to Chenxi Xu.

**Reprints and permission information** is available at <http://www.nature.com/reprints>

**Publisher's note** Springer Nature remains neutral with regard to jurisdictional claims in published maps and institutional affiliations.



**Open Access** This article is licensed under a Creative Commons Attribution 4.0 International License, which permits use, sharing, adaptation, distribution and reproduction in any medium or format, as long as you give appropriate credit to the original author(s) and the source, provide a link to the Creative Commons license, and indicate if changes were made. The images or other third party material in this article are included in the article's Creative Commons license, unless indicated otherwise in a credit line to the material. If material is not included in the article's Creative Commons license and your intended use is not permitted by statutory regulation or exceeds the permitted use, you will need to obtain permission directly from the copyright holder. To view a copy of this license, visit <http://creativecommons.org/licenses/by/4.0/>.

© The Author(s) 2023